NRC Publications Archive
Archives des publications du CNRC

Digital Three-Dimensional Imaging in the Infrared at the National Research Council of Canada

Beraldin, Jean-Angelo; Rioux, Marc; Blais, François; Couvillon, R.A.

NRC Publications Record / Notice d'Archives des publications de CNRC:
https://nrc-publications.canada.ca/eng/view/object/?id=42fb3983-2eae-4300-870a-dbc64bcc95e3
https://publications-cnrc.canada.ca/fra/voir/objet/?id=42fb3983-2eae-4300-870a-dbc64bcc95e3

National Research Council Canada   Conseil national de recherches Canada

Canada

National Research
Council Canada

Conseil national
de recherches Canada

Institute for
Information Technology

Institut de technologie
de l'information

NRC·CNRC

Digital Three-Dimensional Imaging in the Infrared at the National Research Council of Canada ∗

Beraldin, J.-A., Rioux, M., Blais, F., Couvillon, R.A.
July 1994

Canada

Digital Three-dimensional Imaging in the Infrared at the National Research Council of Canada[1]

J.-A. Beraldin, M. Rioux, F. Blais, and R. A. Couvillon
Institute for Information Technology
National Research Council of Canada
Ottawa, Canada K1A 0R6

Abstract

This paper presents work performed at the National Research Council of Canada in infrared range imaging, i.e., from 1.5 μm to 1.8 μm. This region of the spectrum is chosen for eye-safety reasons. Basic concepts explaining the triangulation principle used in NRC prototypes are presented. The requirements for laser source and optics are described in some detail. Laser spot position detection is reviewed in the context of infrared range imaging with actual design examples and detailed calculations of signal-to-noise ratios. These calculations are useful in the early stage of a design. Experimental results show range images taken with the first prototype built at the Institute for Information Technology. A discussion on current developments concentrates on another prototype range camera intended for space applications. The current version of that prototype operates at 0.82 μm and can perform tasks in tracking mode at a refresh rate of 130 Hz (60 targets per second) or in imaging mode at a data rate of 18000 registered 3-D and intensity points per second. The useful range is about 0.5 m to 10 m. For distances greater than 10 m, a time-of-flight unit along with a pulsed-laser source operating at 1.54 μm will be included. The change of operating wavelength will provide a system that is eye-safe and increase the signal to background light rejection for space applications.

Key words: Range imaging, infrared, tracking, time-of-flight, synchronized scanning, position detectors.

1   Introduction

A number of techniques are available for the optical measurement of the shape of the surface of an object. One can distinguish two main categories: feature-based and structured-light projection approaches. In the feature-based approach, 3-D measurements are obtained for specific areas of an object where rapid changes of illumination occur. This method leads to sparse data representation of a surface. With a structured-light approach, a known light pattern is projected onto a scene such that an artificial change of illumination is imposed. Three-dimensional measurements for every pixel in the image are obtained by scanning the light pattern over the desired field of view. The result is an elevation map (range map) of the scene. This approach is favored for the inspection of smooth surfaces for which no natural features are available for a matching algorithm.

Among the many structured-light (non-contact) techniques available to extract 3-D information from a scene, active triangulation is used in applications as diverse as measurement and reproduction of objects, inspection of printed circuit boards, and automatic robot welding[1,2]. An innovative approach, based on triangulation using a synchronized scanning scheme, was introduced by Rioux[3] to allow very large fields of view with small triangulation angles, without compromising on precision. A 3-D surface map is captured by scanning a laser beam onto a scene along two orthogonal directions and collecting the reflected laser light from the scene onto a position detector. Geometric correction of the raw data (laser spot position and angular positions of the scanning mirrors) gives two images in perfect registration: one with x,y,z coordinates and a second with intensity data representing the collected laser power from the scene. The laser beam can be of a single wavelength (visible or infrared) or composed of multiple visible wavelengths for the purpose of measuring the color map of a scene. Most of the prototypes that have been built at our Institute use single wavelength lasers[1], i.e., spanning the spectrum from 0.633 μm to 1.54 μm. One of them can be modified to operate with a white laser. This particular system was demonstrated for museum applications[4].

This paper focuses on the design aspects of a range camera based on triangulation that uses a single wavelength laser source in the short wavelength infrared (SWIR), i.e., 1.5 μm to 1.8 μm, region of the spectrum. The term SWIR will be used throughout this paper to specify this region of the spectrum. Some authors distinguish the near-IR as being the region covered by 0.7 μm to 1.1 μm and the short-wave infrared (SWIR)[5] from 1.1 μm to 3 μm. This laboratory

---

is most interested in range cameras operating in the 1.5 μm to 1.8 μm region because, according to the data published in the American National Standard for the Safe use of Lasers[6] and depending on operating conditions, systems that use lasers that emit in that region of the spectrum are more eye safe than those that emit in the rest of the spectrum, i.e., from 0.18 μm to 1 mm. One should note that between 1.5 μm and 1.8 μm optical materials used in the visible are still adequate and that delivery of the laser beam by a low loss silica optical fibre is possible. Furthermore, another advantage, particularly for space applications, is that the solar spectral irradiance is lower in the SWIR than in the visible.

The optical arrangement of an auto-synchronized range camera is presented in Section 2. The advantages of the auto-synchronized scanning scheme over conventional triangulation are highlighted. The laser spot position detection process is reviewed in detail in Section 3 for two types of position detectors that can satisfy different system requirements. Section 4 addresses design aspects covering the laser source and optics. Experimental results obtained from the first NRC range camera operating at 1.5 μm are presented in Section 5. A discussion follows in Section 6 on a current development of a range camera intended for space applications that will combine a time-of-flight unit for long-range measurements and a pulsed laser source emitting at 1.54 μm. Conclusions appear in Section 7.

2   Active Triangulation Principles

To help explain the optical arrangement used in the prototypes described later in the paper, conventional active triangulation is reviewed and compared with synchronized scanning. The implementation of synchronized scanning as an auto-synchronized camera is shown to have many advantages over conventional triangulation. Also covered are the Scheimpflug condition, diffraction effects, and range noise due to laser speckle.

2.1   Conventional Active Triangulation

The basic geometrical principle of optical triangulation is shown in Fig. 1a. The light beam generated by the laser is deflected by a mirror and scanned on the object. A camera, composed of a lens and a position sensitive photodetector, measures the location of the image of the illuminated point on the object. By simple trigonometry, the x, z coordinates of the illuminated point on the object are calculated. From Fig. 1a,

$$z = \frac{d\, f_0}{p\, +\, f_0\, \tan(\theta)} \tag{1}$$

and

$$x = z\, \tan(\theta) \tag{2}$$

where p is the position of the imaged spot on the position detector, θ is the deflection angle of the laser beam, d is the separation between the lens and the laser source, and f_0 is the effective distance between the position detector and the lens. f_0 is related to the focal length of the lens.

To show some of the limitations of this triangulation method, let us approximate the standard deviation of the error in z, σ_z, as a function of p only[7]. The law of propagation of errors gives

$$\sigma_z = \frac{z^2}{f_0\, d}\, \sigma_p \tag{3}$$

where σ_p is the standard deviation of the error in the measurement of p. The error in the estimate of z is therefore inversely proportional to both the separation between the laser and the position detector and the effective position of the lens, but directly proportional to the square of the distance. Unfortunately, f_0 and d cannot be made as large as desired. d is limited mainly by the mechanical structure of the optical setup and by shadow effects. Furthermore, in the conventional triangulation geometry, the field of view Φ_x of the sensor, assuming the laser beam can scan the whole field of view, is given approximately by

$$\Phi_x \approx 2\, \arctan(\frac{P}{2\, f_0}) \tag{4}$$

where P is the length of the position detector.

Therefore, in the conventional setup, a compromise among field of view, precision of the 3-D measurement, and shadow effects must be considered. A synchronized geometry provides a way to alleviate these tradeoffs.
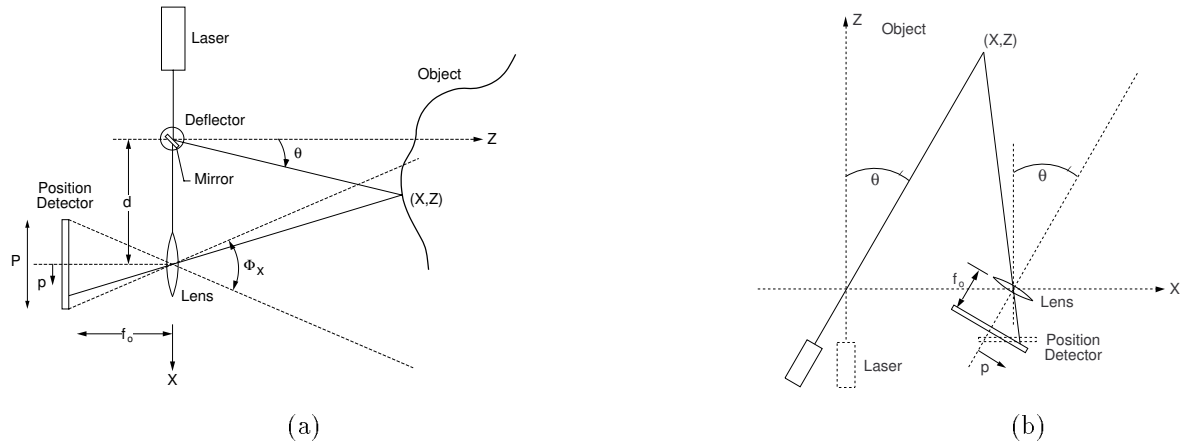
Figure 1: Basic principle of active triangulation: (a) conventional triangulation, (b) synchronized scanner approach.
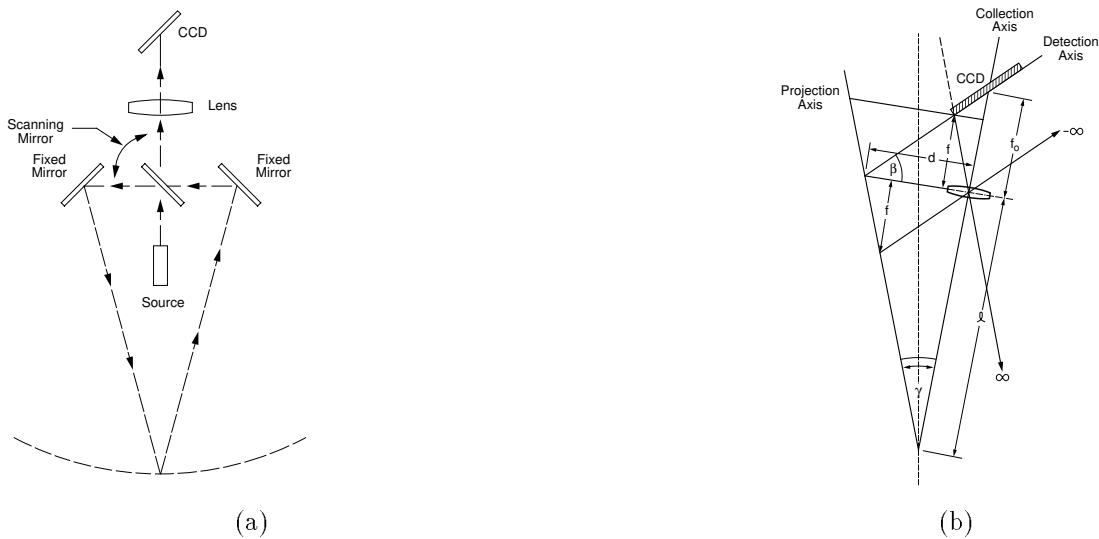

Figure 2: Auto-synchronized scanner approach: (a) with double-coated mirror, (b) Scheimpflug geometry.

2.2 Auto-Synchronized Scanning

Rioux[3] introduced a synchronized scanning scheme, with which large fields of view with small triangulation angles can be obtained without sacrificing precision. With smaller triangulation angles, a reduction of shadow effects is inherently achieved. The intent is to synchronize the projection of the laser spot with its detection. As depicted in Fig. 1b, the instantaneous field of view of the position detector follows the spot as it scans the scene. The focal length of the lens is therefore related only to the desired depth of field or measurement range. Implementation of this triangulation technique by an auto-synchronized scanner approach allows a considerable reduction in the optical head size compared to conventional triangulation methods (Fig. 2a).

Figure 3 depicts schematically the basic components of two types of dual-axis auto-synchronized cameras. In Fig. 3a, 3-D surface maps are obtained by using two oscillating mirrors to scan a laser beam onto a scene, collecting the light that is scattered by the scene in synchronism with the projection mirrors, and finally, focusing this light onto a linear position detector, e.g., photodiode array, charge-coupled device, or lateral effect photodiode. The image acquisition process yields three quantities per sampling interval: two are for the angular position of the mirrors and one for the position of the laser spot on the position detector[8]. For the arrangement depicted in Fig. 3b, the synchronization is achieved with two opposing facets of a polygonal mirror. This kind of arrangement is used mainly in high-speed systems, e.g., video data rates (about 10 mega-samples per second)[9]. The position detector usually chosen for this task is a lateral effect photodiode.
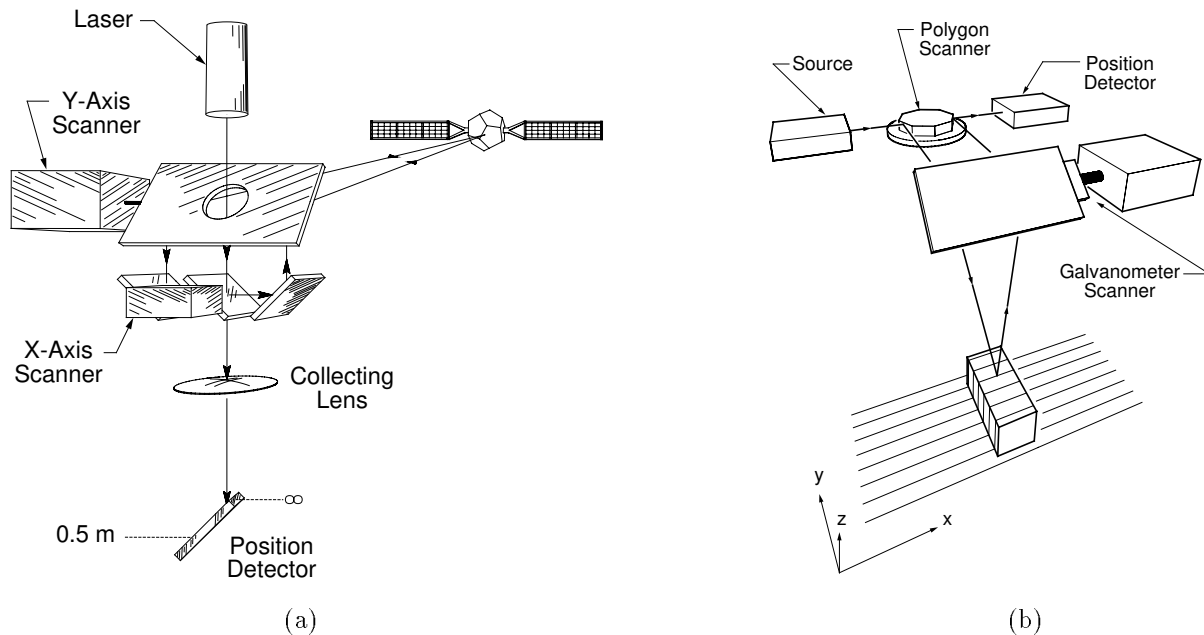
Figure 3: Dual-axis synchronized scanner: (a) dual galvanometers arrangement, (b) polygon and galvanometer arrangement.

2.3 Scheimpflug geometry

As shown on Figs. 2b and 3a, the position detector is tilted compared to the collecting lens. This optical arrangement is known as the Scheimpflug geometry. Figure 2b shows schematically the geometry where the projection and collection axes have been unfolded. The parameters on the figure are the triangulation angle γ, the detector tilt angle β, the lens focal length f, and $f_0 = f\,l/(l-f)$. Triangulation-based range finders can take advantage of the Scheimpflug optical arrangement[10,11]. It is characterized by the fact that the detector axis, the lens principal plane, and the projection axis all intersect at a common point. One of the implications of this optical arrangement is that any point along the projection axis is in focus on the position detector. This property provides a considerable improvement in depth of view. Furthermore, with the Scheimpflug arrangement, the lens aperture can be kept at maximum, thus reducing speckle noise (next section) and improving signal strength[12].

2.4 Diffraction Limit and Speckle

For any laser range imaging device the 3-D sampling properties can be estimated by the accessible number of voxels (volume elements) within a given cubic volume[13]. Using the Gaussian beam propagation formula, one finds

$$\omega(z) = \omega_0 \left(1 + (\frac{\lambda\,z}{\pi\,\omega_0^2})^2\right)^{1/2} \tag{5}$$

where $\omega(z)$ is the radius of the laser beam at a distance z from the beam waist location and λ is the wavelength of the laser source. The beam waist has a radius of ω_0 and is defined as the radius of the $1/e^2$ irradiance contour at the plane where the laser wavefront is flat. Figure 4a shows the propagation of a laser beam within the volume of interest. Then, if the depth of field a is defined following the Rayleigh criterion,

$$a = 2\,\frac{\pi\,\omega_0^2}{\lambda} \tag{6}$$

Such a constraint imposed by the diffraction limit leads to the following relationship.

$$\omega_0 = (\frac{\lambda\,a}{2\,\pi})^{1/2} \tag{7}$$

4

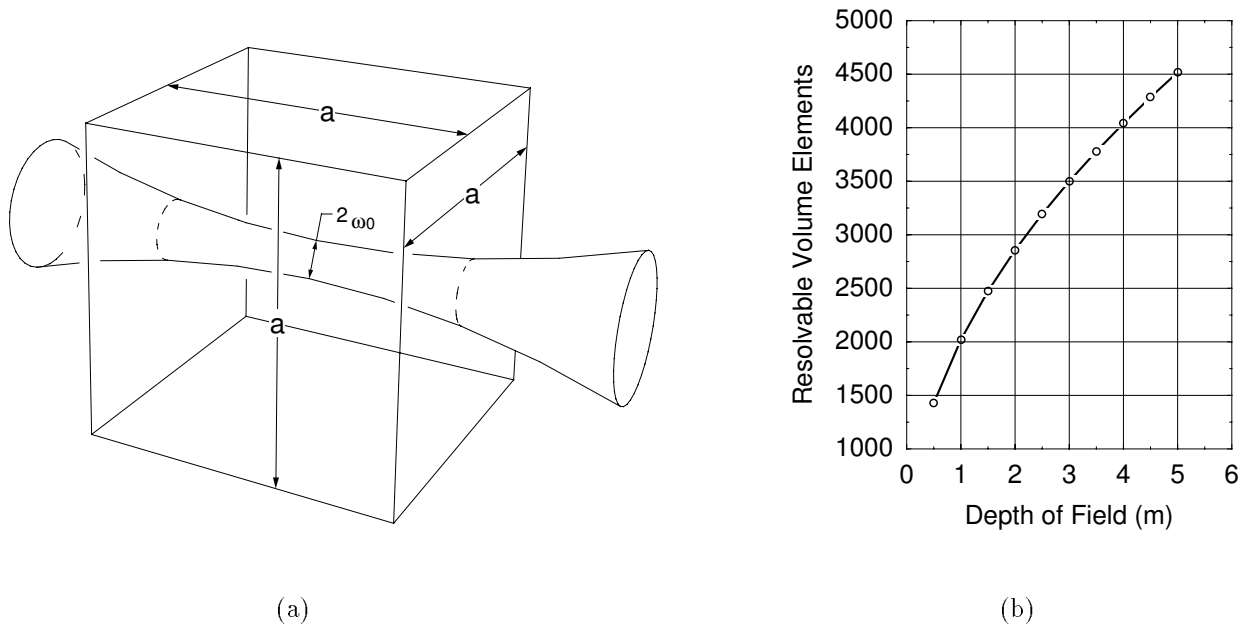(a)   (b)

Figure 4: Gaussian beam: (a) propagation in space, (b) resolvable volume elements for $\lambda = 1.54\ \mu$m.

The maximum number of resolvable volume elements (V_{F}) along each axis within the volume of interest is

$$V_{\mathrm{F}} = \frac{2\,\pi\,\omega_0}{\lambda} = \left(\frac{2\,\pi\,a}{\lambda}\right)^{1/2} \tag{8}$$

Figure 4b shows a graphical representation of this function for $\lambda = 1.54\ \mu$m. As an example, within a cube of 3 m on a side, one has access to 3500^3 voxels.

Laser speckle is an important issue with range cameras because in most cases it will impose a lower limit on their range measurement precision σ_{z}. The range precision in a synchronized scanner is in practice limited by the laser speckle impinging on the position detector. Speckle manifests itself on the measurement of the laser spot position on the detector. The value of σ_{p} will depend on the type of detector that one chooses for a camera. With current technology, a high-speed range finder will use a continuous response detector like a lateral effect photodiode. Beraldin *et al.*[9] describe a system that uses such a position detector to generate registered range and intensity data at 10-Mega samples per second. The value of σ_{p} can, for this kind of system, be approximated with the noise model presented in[14] for low collected power. For high collected power, the contribution of laser speckle for this detector is described in[15]. Usually, range finders based on a discrete-type detector like self-scanned photodiodes arrays and CCDs provide data with higher levels of accuracy than those based on a continuous response detector[7] but at a reduced data rate. For this position detector, the laser spot position measurement uncertainty has been modeled in[15] when speckle noise dominates. Both position detectors are covered in more detail in the following section.

3 Laser Spot Position Detection

This section examines in more detail the two most common position detectors used to extract the location of the laser spot in an active range camera, i.e., discrete and continuous response detectors. The former is implemented with a linear array of photodiodes and the latter with a lateral effect photodiode. The operation, the speckle noise, the bandwidth requirement, the dynamic range (noise level) and a design example are supplied for each detector.

3.1 Discrete Response Detector: Linear Array of Photodiodes

3.1.1 Operation

Recent advances in InGaAs materials have made possible the fabrication of commercial SWIR detector arrays that operate at room temperature[16]. Commercial detector arrays are composed of an array of photodiodes made of InGaAs
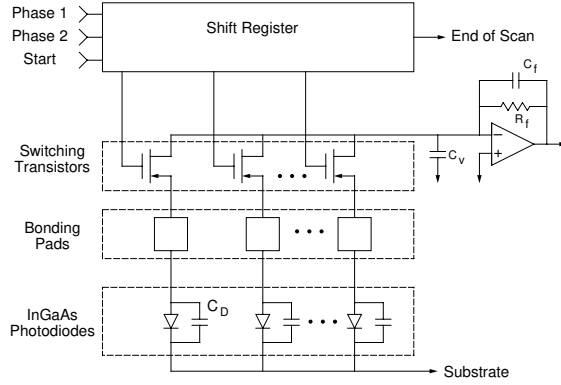
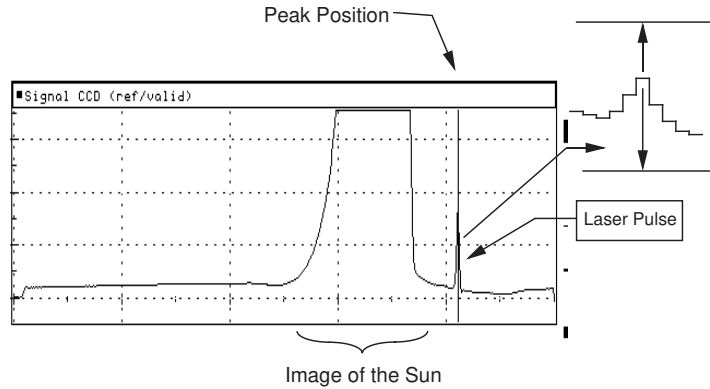Figure 5: Equivalent circuit of detector array.

Figure 6: Laser spot detected even with partly saturated detector.

that are wire-bonded to a MOSFET-based multiplexer made of silicon. The width of the active area of one photodiode varies from 25 μm to about 50 μm and height from 100 μm to about 500 μm. Array lengths vary between 64 and 1024 photodiodes. These arrays operate on the principle of charging the photodiodes junction capacitance with a suitable bias voltage present on the video line during the sequential read-out and letting the impinging light discharge (by photon-generated carriers) the junction capacitance. This video line connects all the photodiodes through a MOSFET (as shown on Fig. 5). Finally, an external pre-amplifier performs the charge-to-voltage conversion. Newer arrays combine an amplifier with each photodiode[17]. Their output is then multiplexed. The maximum clock speed is about 5 MHz. The output of the detector is a stream of pulses where the envelop is a function of the laser spot distribution. The time occurrence of the peak on the video signal is directly related to the geometrical position of the laser spot. For example, a 512-photodiode array clocked at 5 MHz yields a maximum spot position measurement rate of about 9.76 kHz, if it is assumed that the laser position can be extracted at a pixel rate of 5 MHz. The circuit described below was specifically designed for that purpose.

Sub-pixel interpolation is performed by a digital finite impulse response (FIR) filter containing a derivative stage[18]. The output of this filter is used to interpolate the zero-crossing of the signal. A validation step is added to eliminate false detections. Maximum peak position extraction rate is achieved by allowing the imaged laser spot to extend over a number of photodiodes and interpolation. The operator provides good attenuation of low and high frequency noise and especially of the frequency components induced by the clocks used to address and read each photodiode of the array. Immunity to interfering light sources (artificial or natural, e.g., the sun) or even from multiple reflection of the laser source itself is critical for achieving a robust peak position detector. The method implemented here for a linear array of photodiodes can still operate even with a partly saturated section on it, as shown on Fig. 6. Section 4.3 provides more information on the occurrence of this condition.

ω_0 (μm)	B_s (MHz)
100	1.33
150	0.83
200	0.66
250	0.53
300	0.44

Table 1: Bandwidth requirement for a 512-element InGaAs array clocked at 5 MHz and with a pixel width of 50 μm.

3.1.2 Speckle

Baribeau and Rioux[12] predicted that speckle noise for such a position detector and peak finding method behaves like a Gaussian process and the estimated rms fluctuation of p determined by such noise is given by

$$\sigma_\text{P} = \frac{1}{\sqrt{2}} \frac{\lambda\, f_0}{D\, \cos(\beta)} \frac{1}{\sqrt{\pi}} \tag{9}$$

where λ is the wavelength of the laser source, f_0 is the effective position of the imaging lens, D is the lens diameter, and β is the tilt angle of the position detector. Let us take a design example: with $f_0 = 110$ mm, $D = 20$ mm, $\lambda = 1.54\,\mu$m, and $\beta = 55°$, one gets $\sigma_\text{P} = 5.89\,\mu$m or 1/8.5 of detector pixel (pixel width = 50 μm).

To augment the precision on p, one cannot strictly average a number of spot position measurements, because the imaged speckle pattern does not change when multiple samples of the same surface patch are measured. For a given surface patch the macroscopic structure does not change. Spatial averaging is the only solution to reduce σ_p. Dremel *et al.*[11] propose introduction of spatial averaging in the object plane or in the pupil plane of the imaging lens. The first method is inherent to the synchronized scanner. When a constant depth surface is scanned, the image of the laser spot remains almost stationary on the position detector[12]. Because a linear array of photodiodes responds to the integral of the light pattern during a measurement interval, the net result is a four-fold improvement on the precision σ_P, i.e., $\sigma_\text{P} = 1.47\,\mu$m or 1/34 of a pixel. For other surface orientations, this factor varies between 1 and 4.

3.1.3 Bandwidth Requirement

Prior to digitizing the laser spot, an anti-aliasing filter with linear phase is necessary. The choice of the filter bandwidth is a tradeoff among noise bandwidth, aliased components, and accurate reproduction of the envelope of the laser spot. The criterion used is that the filter should introduce less than 1 dB attenuation at the cutoff frequency for a minimum spot size of $\omega_0 = 100\,\mu$m ($p_\text{w} = 50\,\mu$m). Hence, the bandwidth requirement of the detection chain (charge-to-voltage converter and anti-aliasing filter) is given approximately by

$$B_\text{s} \approx \frac{2\,\sqrt{\ln 2}}{\pi} f_\text{s} \frac{p_\text{w}}{\omega_0} \tag{10}$$

where B_s is the required -3 dB system bandwidth, f_s is the pixel clock rate, p_w is the pixel width, and ω_0 is the spot radius at $1/e^2$. The envelope of the laser spot is modeled by a Gaussian distribution. According to experimental measurements, this model is found sufficient for design purposes. Table 1 shows the bandwidth requirement for typical spot sizes with a commercial 512-element InGaAs array with $p_\text{w} = 50\,\mu$m.

3.1.4 Dynamic Range and Noise Sources

The dynamic range of an array of photodiodes is defined as

$$DR_\text{Array} = \frac{Q_\text{T}/q_\text{e}}{(\overline{n_\text{T}^2})^{1/2}} \tag{11}$$

where Q_T is the total equivalent charge collected on a photodiode (saturation charge), q_e is the electronic charge and $(\overline{n_\text{T}^2})^{1/2}$ is the equivalent input referred noise in electrons. The saturation charge of a pixel, assuming the capacitance of the junction varies with the reverse voltage across it, is given by

$$Q_\text{T} \approx 2\,(V_\text{bi}\, V_\text{r})^{1/2}\, C_\text{j0} \tag{12}$$

7

where V_{bi} is the built-in voltage for InGaAs, V_r is the maximum reverse bias across the photodiode, and C_{j0} is the junction capacitance at zero bias[19].

With linear arrays of photodiodes, one can distinguish two sources of interference: (1) those that are stationary for a fixed temperature and clock rate and (2) those that are random in nature. The former is often called fixed-pattern noise and includes among other things[19]

- Dark current variability across the array,

- Sensitivity variation between photodiodes,

- Reading clock feedthrough.

Random noise sources[20] are composed of

- Photon shot noise of the incident light,

- Shot noise of the dark current,

- Reset noise of the pixels in the array,

- Current and voltage noise of the pre-amplifier.

Two other sources of noise are identified in the literature: the amplifier glow noise[21] and popcorn noise[22]. These two sources of noise are not covered here.

The equivalent input referred noise (in electrons) due to the random noise sources is

$$\overline{n_T^2} = \frac{(i_{ph} + i_d)}{q_e} \frac{N}{f_s} + \frac{1}{q_e^2} k\, T\, C_T + \frac{C_f^2 \, \overline{e_n^2}}{q_e^2} \tag{13}$$

where $i_{ph} = P_{det}\, \mathcal{R}$ is the incident light (laser and background), i_d is the averaged dark current, N is the number of pixels (photodiodes), P_{det} is laser power collected on one photodiode before saturation is reached, and $\mathcal{R}$ is the photodiode responsivity at the wavelength of interest. The dark current has a strong dependence on temperature. It is halved for every decrease of 8°C. C_T is the total capacitance that is reset to the video-line bias. It includes the photodiode junction and parasitic capacitance and the video-line to clock-lines capacitance[20]. The integrated noise (over B_s) due to the charge amplifier of Fig. 5 is found by computing the voltage noise at the output of the amplifier and then with the gain factor (C_f) converting from voltage to charge, i.e.,

$$\overline{e_n^2} = B_s\,(\overline{i_a^2}\, R_f^2 + 4\,k\,T\,R_f) + B_1\,\overline{e_a^2} + \left(\frac{B_s^3 - B_1^3}{3\,B_1^2}\right)\overline{e_a^2} \tag{14}$$

where $\overline{i_a^2}$ and $\overline{e_a^2}$ are, respectively, the amplifier current and voltage noise spectral densities, R_f and C_f are the feedback resistance and capacitance, respectively, and $B_1 \leq B_s$ is the frequency of the zero introduced in the noise gain of the amplifier, $B_1 \approx (2\,\pi\,R_f\,(C_v + C_D))^{-1}$. C_v and C_D are the video line and photodiode capacitances, respectively. The temperature is given by T and k is Boltzmann's constant. Usually, these noise sources include flicker noise (noise with $1/f$ type distribution). Here, it is omitted because the derivative term in the FIR filter of the peak detector eliminates that noise component. Furthermore, fixed-pattern noise should be removed for the different operating conditions of the array, e.g., temperature and integration time, to improve operation in lower signal-to-noise ratios (SNR). Usually, for high SNR, the effect of the random noise and the quantization noise of the peak detector[7] on the measurement of p are swamped by speckle noise.

3.1.5 Example

Table 2 presents a design example for an InGaAs photodiode array composed of $N = 512$ photodiodes, which is read at 5 MHz and is connected to a typical charge pre-amplifier. The dynamic range is equivalent to 14 or 15 bits of an analog-to-digital converter. Converters with 14-bit resolution are readily available at 5 MHz. A closer look at the noise contribution of the different sources shows that 94.5% (ratio of variances) comes from the reset noise. Therefore, one can take advantage of a technique called correlated double sampling (CDS) to reduce substantially this noise source[19]. Correlated double sampling, however, doubles the amplifier noise power component (14). Nevertheless, the dynamic range would still be about 2×10^5, i.e., almost 18 bits. Correlated double sampling is now integrated directly in the multiplexers used with InGaAs linear arrays[17].

SPECIFICATION	VALUE
N	512
f_s	5 MHz
Pixel width p_w	50 μm
Pixel height p_h	100 μm
Spot size (ω_0)	125 μm
V_r	-5 V
T	300 K
I_d	8 pA
C_j	2.5 pF
R_f	5.6 kΩ
C_f	2.7 pF
i_a	0.1 pA/$\sqrt{Hz}$
e_a	5 nV/$\sqrt{Hz}$
B_s	1 MHz
Saturation Charge per pixel	$40 \times 10^6\,\bar{e}$
Saturation Power for ω_0	500 nW
Noise Charge per pixel	$1600\,\bar{e}$
Noise Power for ω_0	20 pW
Dynamic Range	25000

Table 2: Design example for 512-element InGaAs array.

3.2 Continuous Response Detector: Lateral Effect Photodiode

3.2.1 Operation

A lateral effect photodiode (LEP) sensitive to 1.54 μm has been demonstrated[23]. Figure 7 illustrates the basic structure of a *pin* type InGaAs/InP single-axis position detector along with two transimpedance amplifiers. Carriers produced by light impinging on the device are separated in the depletion region and distributed to the two sensing electrodes according to Ohm's law. Assuming that all drifts have been canceled in the electronics then the normalized position of the centroid of the incident light distribution is given by

$$p = \frac{i_2 - i_1}{i_1 + i_2},\ p \in [-1, 1] \tag{15}$$

where i_1 and i_2 are measured with transimpedance amplifiers. The actual position on the detector is found by multiplying the above equation by $L/2$ where L is the distance between the two sensing electrodes. The total photocurrent i_{ph} is

$$i_{\text{ph}} = i_1 + i_2 = P_{\text{det}}\mathcal{R} \tag{16}$$

where P_{det} is the incident light power and $\mathcal{R}$ is the responsivity of the photodetector, which is in the order of 0.7 A/W.

The frequency response of a junction photodiode can be affected by two main types of phenomena: (1) transit-time effects, which arise from the delay between the absorption of the incident light and the separation of photo-excited electron-hole pairs and (2) the inherent electrical characteristics of the position detector, i.e., the series resistance of the diode and its junction capacitance. If the maximal required bandwidth for range finding applications is less than 4 MHz, the distributed resistance and capacitance of the lateral effect photodiode and the transimpedance amplifiers dominate the transient behavior of the position detector[14]. One can estimate the bandwidth f_{LEP} of a lateral effect photodiode as

$$f_{\text{LEP}} = \frac{\pi}{2} \frac{1}{R_p C_j} \tag{17}$$

where R_p is the inter-electrode resistance and C_j the junction capacitance. Equation (17) is a first-order approximation and applies only when the load impedances are equal to zero. An inter-electrode resistance of 5.6 kΩ and a junction
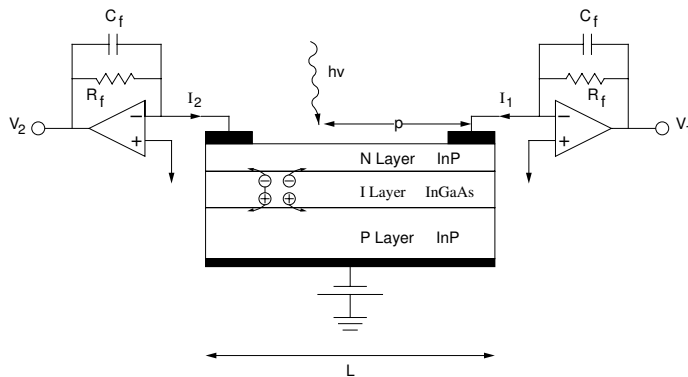
Figure 7: InGaAs lateral effect photodiode.

capacitance of 39 pF at a bias of -5 V were measured for the prototype lateral effect photodiode[23]. Hence, the maximum bandwidth of the present detector is 7.2 MHz, which is quite adequate for video-rate range cameras[24]. A complete analysis of the effect of transimpedance amplifiers on the transit behavior of the detector appears in[14].

3.2.2   Speckle

Baribeau and Rioux[12] predicted that speckle noise for a centroid detector behaves like a Gaussian process and the estimated rms fluctuation of p determined by such noise is given by

$$\sigma_{\rm p} \,=\, \frac{1}{\sqrt{2}} \, \frac{\lambda \, f_0}{D \, \cos(\beta)} \, \frac{1}{\pi} \tag{18}$$

where λ is the wavelength of the laser source, f_0 is the effective position of the imaging lens, D is the lens diameter, and β is the tilt angle of the position detector. According to this equation, $\sigma_{\rm p}$ for a centroid detector is $\sqrt{\pi}$ better than one that uses a FIR derivative filter[7]. But, in practice, most systems that operate at high data rates ($\geq$100 kHz) use a lateral effect photodiode and therefore thermal and quantum noise sources, not speckle noise, will limit the detection process.

3.2.3   Bandwidth Requirement

The required system bandwidth is determined by the size of the laser spot and the speed at which it scans a feature on a scene. It is customary to compute the system bandwidth or equivalently the rise time of the collected light from the scene as the laser spot moves over a transition in reflectance. Again, one assumes the laser spot distribution on the detector to be Gaussian with dimension ω_0. The spot size as determined by diffraction is related to the standard deviation of a Gaussian distribution, σ_0, by $\omega_0 \,=\, 2\,\sigma_0$. The resulting normalized time response waveform is given as

$$F(t) \,=\, \frac{1}{2} \, {\rm erfc}\big(\frac{x_{\rm t} - (x_0 + v_{\rm s}t)}{\sqrt{2}\sigma_0}\big) \tag{19}$$

where $x_{\rm t}$ is the position of the reflectance transition, x_0 is the initial position of the centroid of the laser spot, $v_{\rm s}$ is laser spot speed on the scene, and t is the time variable. From this equation, one can compute the 10% to 90% rise time and hence the system bandwidth requirement.

3.2.4   Dynamic Range

The dynamic range of a position detector based on a lateral effect photodiode is defined as

$$DR_{\rm Lep} \,=\, \frac{i_{\rm sat}}{(\overline{i_{\rm n}^2})^{1/2}} \tag{20}$$

where $i_{\rm sat}$ is the saturation current and $(\overline{i_{\rm n}^2})^{1/2}$ is the total equivalent current noise referred to the input of the amplifiers.

10

SPECIFICATION	VALUE
LEP length	10 mm
LEP height	200 μm
Spot size (ω_0)	50 μm
V_{r}	-5 V
T	300 K
I_{d}	400 nA
C_{j}	39 pF
R_{p}	5.6 kΩ
R_{f}	220 kΩ
i_{a}	0.6 pA/$\sqrt{Hz}$
e_{a}	4.5 nV/$\sqrt{Hz}$
B_{s}	200 kHz
Saturation Current	1 mA
Saturation Power	1.43 mW
Noise Current	1.0 nA
Noise Power	1.43 nW
Dynamic Range	10^6

Table 3: Design example for InGaAs/InP lateral effect photodiode.

Figure 7 is used to compute the effect of the different input noise sources on the output signals. The result is given below

$$\overline{i_{\mathrm{n}}^2} = \overline{e_{\mathrm{a}}^2}\left[\left(\frac{1}{R_{\mathrm{f}}} + \frac{1}{R_{\mathrm{p}}}\right)^2 + \left(\frac{1}{R_{\mathrm{p}}}\right)^2\right] + 4\,K\,T\,B_{\mathrm{s}}\left(\frac{1}{R_{\mathrm{f}}} + \frac{1}{R_{\mathrm{p}}}\right) + \overline{i_{\mathrm{a}}^2} + 2\,q_e\,B_{\mathrm{s}}\left(\frac{i_{\mathrm{d}}}{2} + i_{\mathrm{ph}}\right) \tag{21}$$

where $(\overline{e_{\mathrm{a}}^2})^{1/2}$ and $(\overline{i_{\mathrm{a}}^2})^{1/2}$ are the pre-amplifier integrated (over B_{s}) input noise voltage and current noise, respectively, R_{f} is the feedback resistor value, R_{p} is the positioning resistor value, and i_{d} is the dark current.

3.2.5 Example

Table 3 presents a design example for the InGaAs/InP lateral effect photodiode built to NRC specifications. The following design parameters were used for the camera described in Section 5. The dynamic range is equivalent to 20 bits of an analog-to-digital converter. Converters with 16-bit resolution are available at 1 MHz. Making use of the full dynamic range of an LEP poses quite a challenge to system designers[9,25]. A closer look at the noise contribution of the different sources shows that 62% (ratio of variances) comes from the thermal noise of R_{p} and 28% from the voltage noise of the amplifiers. Therefore, the noise level could be reduced by increasing R_{p} and by selecting an amplifier with a lower voltage noise. But, unfortunately, the dynamic range would not increase accordingly because the saturation current is also a function of R_{p}.

4 Sources of Light and Eye Safety Issues

This section surveys the different laser sources for the SWIR, in particular for the region 1.5 μm to 1.8 μm. A summary on maximum permissible exposures pertinent to eye safe laser range cameras operating in that region of the spectrum is tabulated and compared to other common wavelengths. The optical efficiency of a range camera and the solar spectral irradiance are covered also.

4.1 Laser Sources for the SWIR

Two categories of infrared laser sources that are quite adequate for range cameras are emerging, i.e., solid-state lasers and laser diodes. Numerous pulsed and continuous wave (cw) laser sources emitting in the SWIR (1.5-3 μm) are being
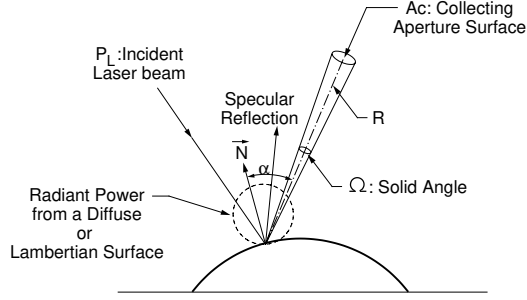
Figure 8: Effect of surface reflectivity on the received laser power.

developed for applications including eye safe laser radar systems and medical systems. Solid-state lasers have received a lot of attention in recent years[26,27], due in part to a reduction of the cost of high-power laser diodes as a pump source. Commercial lasers with adequate power levels for range cameras have started to appear on the market. At the Institute for Information Technology, two types of solid state lasers were developed for ranging applications[28] and another for optical time domain reflectometers[29]. Laser diodes have also started to break ground in the high-power arena (above 300 mW)[30].

4.2 Optical Efficiency

The estimation of the required laser power is an important step in the design process. From Fig. 8, the equation relating the power impinging on the position detector P_{det} to the laser power P_{L} for a diffusive surface[31] is

$$P_{\text{det}} = P_{\text{L}} \ \left(\frac{T \ \ \rho \ \ \Omega \ \ \cos \alpha}{\pi} \right) \tag{22}$$

where T is the transmission coefficient accounting for the focusing and collecting optics, ρ is the diffuse reflectance coefficient, and α is the angle between the normal of the surface being measured and the solid angle Ω subtended by the collecting aperture. The solid angle can be approximated for R much larger than the aperture diameter by

$$\Omega \simeq \frac{A_{\text{c}}}{R^2} \tag{23}$$

where A_{c} is the area of the collecting aperture and R is the distance between the surface being illuminated by the laser beam and the collecting aperture.

4.3 Solar Spectral Irradiance

In a space environment, a range camera will have to operate under a high level of solar irradiance. Therefore, it is imperative that the camera be designed or equipped with sun blocking capabilities. A range camera based upon a synchronized scanner technique has an inherent way to reduce spurious light, i.e., the instantaneous field of view is much smaller than the total field of view of the camera. Another way to reduce solar irradiance is to use an interference filter tuned to the laser wavelength. Furthermore, if ones looks at the solar spectral irradiance outside the atmosphere[32], a ratio of 5.8 is found between the solar spectral irradiance at 0.632 μm and 1.54 μm. Finally, the last method of solar interference rejection is due to the Scheimpflug condition (see Section 2.3). Figure 9 shows an example of the focusing of the sun on a position detector for $\beta = 55°$, $D = 20$ mm, and $f = 100$ mm. Because of this optical arrangement, the sun, located at infinity, is always focused in the focal plane of the lens; thereby its image will spread out on the position detector except at the intersection of the focal plane and the detector. This last situation could confuse the peak detection process. For a discrete response detector as specified in Table 2, the collected power per nanometre of bandwidth of an interference filter is 25 μW (transmission of optical path is 30%). Hence, at $z- > \infty$, a pixel will collect 79.6 nW, which is less than the saturation level of 90 nW per pixel. At p corresponding to $z = 0.5$, the collected power is 25 times less intense. It can be concluded that, when the sun appears in the instantaneous field of view of the
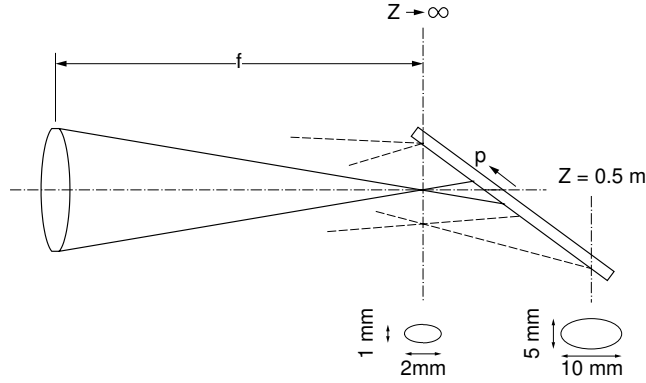
12

Figure 9: Image size of the sun on a tilted detector.

camera, the dynamic range of the detector will be reduced for objects located at longer distances and increased as the object gets closer to the camera.

4.4 Maximum Permissible Exposure

For applications requiring eye safety, maximum permissible exposure (MPE) is very important. It varies with wavelength and operating conditions of a system. The MPE is defined as the level of laser radiation to which a person may be exposed without hazardous effect or adverse biological changes in the eye or skin[6]. This standard also contains many provisions for the safe use of laser systems and for the preparation of the environment surrounding laser systems. Before attempting any experiment that require eye safety, it is recommended to consult the ANSI standard[6] and to get proper certification for commercial use of such a laser system. For example, fractions of a milliwatt in the visible spectrum are sufficient to cause eye damage, since the laser light entering the pupil is magnified, at the retina, through the lens, by a factor of roughly 10^5 (intra-beam viewing). At longer wavelengths, however, strong absorption by water present in the eye serves to reduce optical power reaching the retina, thus increasing the damage threshold. Water absorption is the mechanism by which the laser light is stopped at the surface of either the skin or the eye. From the absorption coefficient of water at 1.5 μm, an e-folding distance of 0.6 mm is found, which means that any damage that could occur will always be surface effects and not damage to the retina. From Table 4, at 1.54 μm the recommended single-pulse threshold energy for eye damage is roughly 10^4 times greater than it is at the visible wavelength ($\lambda = 0.632$ μm). For longer exposure, Table 5, the recommended threshold power factor is down to 10^3. The ANSI standard for eye safety takes into account that some laser light at 1.54 μm is transmitted though the cornea and reaches the lens. The rest is absorbed by the vitreous body of the eye.

Considering that the noise levels of InGaAs position detectors are about the same as that of silicon-based position detectors and that scattering strengths of rough surfaces are similar at 1.54 μm and in the visible region, there is potential for signal improvement of 30-40 dB (optical) if 1.54 μm is chosen instead of the visible for making eye-safe range measurements. Noise level of InGaAs position detectors was covered in Section 3. Scattering properties at 1.54 μm for a range of surfaces including good diffusers, e.g., Al_2O_3 powder on glass and on Macor substrates, and, very adsorptive surfaces such as human skin were compared[33] with measurements made at 0.514 μm.

5   Infrared Range Camera Prototype

5.1   Position Detector

For this infrared range camera, the average spot speed is about 420 m/s. For a spot size $\omega_0 = 250$ μm in the scene, the 10% to 90% rise time is about 1.5 μs (19). This rise time is equivalent to a bandwidth of 230 kHz for a linear phase filter of order six. A data rate of 600 kHz was chosen for the 12-bit analog to digital converters. Let us assume $T \simeq 50\%$, $\rho/\pi = 0.05$ (skin), $\Omega \simeq 9 \times 10^{-3}$, and $\alpha = 45°$. Then, for a standoff distance of 650 mm and for an equivalent power on the analog-to-digital converter of 2 μW (for 10 bits of precision σ_z), $P_L \approx 15.5$ mW (22). This value is within reach of the laser source used. It is worth noting that range precision for this camera varies almost linearly with the collected laser power[33]. From Table 3 and for a collected power of 0.2 μW, the range precision is about 7 bits.

Wavelength (μm)	Exposure Duration (s)	Single-Pulse MPE (J/cm^2)	Eye Aperture Diameter (mm)
0.632	10×10^{-9}	0.50×10^{-6}	7
0.820	10×10^{-9}	0.86×10^{-6}	7
1.060	10×10^{-9}	5.0×10^{-6}	7
1.540	10×10^{-9}	1.0	1
2.000	10×10^{-9}	0.1	1

Table 4: MPE for Ocular Exposure (Intrabeam Viewing) to a Laser Beam (single pulse mode)[6].

Wavelength (μm)	Exposure Duration (s)	MPE (W/cm^2)	Eye Aperture Diameter (mm)
0.632	10^4 to 3×10^4	16.98×10^{-6}	7
0.820	10^3 to 3×10^4	0.556×10^{-3}	7
1.060	10^3 to 3×10^4	1.6×10^{-3}	7
1.540	10 to 3×10^4	0.1	3.5
2.000	10 to 3×10^4	0.1	3.5

Table 5: MPE for Ocular Exposure (Intrabeam Viewing) to a Laser Beam (long period)[6].

5.2 The Laser Scanner

Figure 10a shows a photograph of the prototype[33] that has been modified to operate at 1.5 μm. The scanning head consists of a six-faceted pyramidal mirror that provides the x-axis scanning (see Fig. 3), a flat mirror driven by a stepping motor providing the y-axis scanning, and projection and detection units. The following modifications were also made: (1) replacement of the diode laser by the fibre laser output and (2) replacement of the silicon lateral effect photodiode by an InGaAs unit (Section 3.2). No change in the optical elements was needed, only minor adjustments for the focusing of both the projection and detection units to compensate the effect of the index of refraction change which occurs by shifting the wavelength from 0.820 to 1.5 μm. The sampling rate of the position sensor remained at 600 kHz using the existing hardware. The 1.5 μm fibre laser delivers up to 80 mW through a 50-m length of telecommunication grade single-mode fibre. Of this light, 40 mW is projected into the scene owing to losses in the camera projection optics. This amount is sufficient for the targeted range resolution.

The recommended maximum permissible exposure (MPE)[6] at 1.5 μm wavelength, considering that the laser beam spends 2.2×10^{-4} s impinging on the pupil of the eye, is

$$\text{MPE} = 1.0 \, \text{J/cm}^2 \tag{24}$$

To respect this exposure limit, the CW scanning laser power must be less than 35.6 W for a recommended eye aperture of 0.1 cm. This is about 10^4 larger than the corresponding limit calculated for an He-Ne wavelength of 0.633 μm and well below the maximum power available from current infrared laser sources.

5.3 Experimental Results

Figure 10b-c shows a recording on a human subject that has been taken with an incident power level of 40 mW ($\sim 900\times$ less than the MPE). Figure 10b is the 1.5 μm intensity image and Fig. 10c is the registered range image. A grey level coding is used to display range information. White is for surface elements close to the camera whereas black is for elements located at the furthest extreme of the volume of measurement. On the eye, it is interesting to note that the water layer on the conjunctiva (sclera) is not thick enough to prevent scattering and good reading of the shape occurs up to the edge of the cornea. Image acquisition time is of the order of 1 s. The profiles from each of the six facets are averaged to decrease the scanning noise introduced by the facet-to-facet angular tolerances. The volume of view
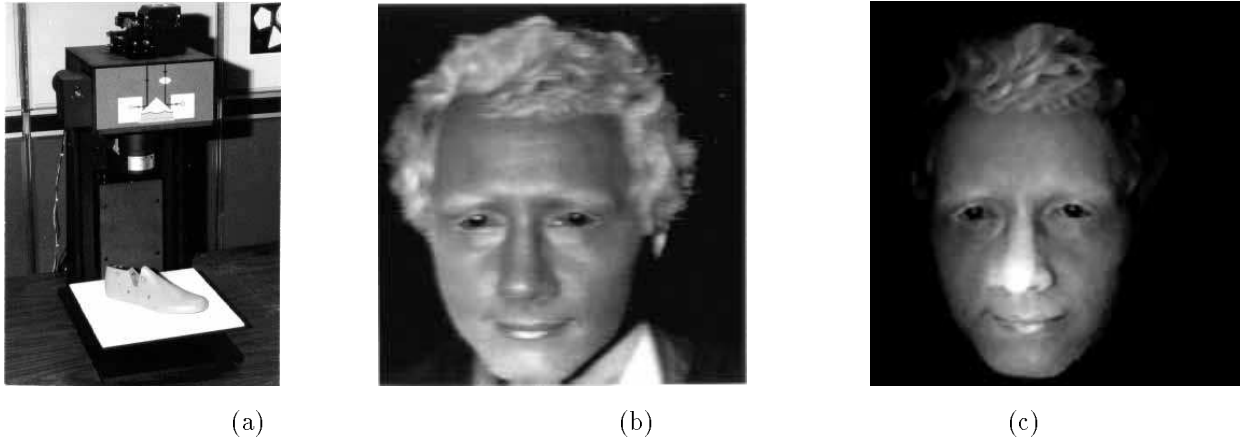
(a)   (b)   (c)

Figure 10: Experimental results for $\lambda = 1.5$ μm: (a) laser scanner prototype, (b) intensity image, (c) range image.

is 250 mm × 250 mm × 150 mm along the x, y, and z axes, respectively. The sampling in the x and y axes is of the order of 1 mm whereas the resolution along the z axis is of the order of 36.6 μm (1 part in 4096). The range precision σ_z was estimated at about 250 μm on skin.
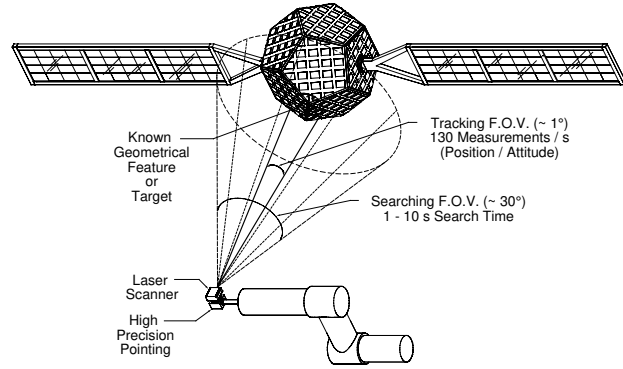
6   Current Developments: Range Camera for Space Applications

A photograph of this range camera is shown in Fig. 11a and a schematic representation of the optical arrangement appears in Fig. 3a. The camera operates in either a variable resolution mode or a raster type mode at a maximum data rate of 18000 points per second. In the variable resolution mode, as illustrated in Fig. 11b, the laser scanner tracks targets and geometrical features of objects located within a field of view of 30° × 30° and with a range from about 0.5 m to 100 m. For objects located at distances greater than 6 m, cooperative targets on their surfaces are required for good signal-to-noise ratio. The range camera uses two high-speed galvanometers to steer the laser beam to any spatial location within the field of view of the camera. A compact dual-galvanometer controller was designed specifically for this task. Each axis can be addressed by more than 16 bits with a step response of 1.8 μs over wide angles even though the mirrors are quite large. This increase in speed and versatility over the original manufactured controller allows the generation of Lissajous patterns for tracking of objects at a refresh rate of up to 130 Hz (60 targets per second)[34]. The raster mode is used primarily for the measurement of registered range and intensity information of large stationary objects[34]. Figure 12 shows an image of a quarter-scale model (located at the National Research Council) of the cargo bay of the Space Shuttle Orbiter. The scale model measures 4.33 m by 1.42 m by 0.6 m. Although, it was digitized to a spatial resolution of 2048 × 4096, the figure displays a re-interpolated image on a grid of 512 × 1024.

The current version of this range camera operates at $\lambda = 0.82$ μm and at a laser power of 150 mW. This makes its operation hazardous to the naked eye. Work has started to enhance the system to include eye safety and long-range capabilities. The requirement for eye safety will be fulfilled by operating at $\lambda = 1.54$ μm and by changing the silicon-based discrete position detector by an InGaAs unit. That position detector is described in Section 3.1. With the data presented in Sections 3.1 and 4.3, the required laser power to saturate the detector for a surface with $\rho = 1$ at a distance of $z = 1.0$ is about 10 mW. At $z = 10$ m, the required power is in the order of 1 W. The range camera will be further enhanced by the addition of a time-of-flight (TOF) unit that will take over for $z > 10$ m. Incidently, a TOF unit provides a range precision that is fairly constant with distance as opposed to a triangulation-based camera where range precision is a function of distance (excluding collected power effects). The transition in precision occurs at about 10 m. This TOF unit can be merged easily in the current range camera. From Fig. 3a, a beam splitter can be positioned in the collecting path of the laser beam just above the position detector. And for distances over 10 m, an avalanche photodiode will pick up the returned signal generated from a pulsed laser source. A proof of concept unit has been recently built to demonstrate the technique. At a data rate of 10000 points per second, the required energy per pulse for a surface with $\rho = 1$ at a distance of 1 m is 2 μJ (including 50% loss of beam splitter). At 10 m, the energy is about 200 μJ. These power or energy levels are achievable with current commercial laser technology. Furthermore, these levels are also well below their respective MPEs when the laser beam is scanned over a scene (see Section 4.4)[6].

15

Figure 11: Range camera: (a) photograph, (b) real-time tracking of satellite.

7 Conclusion

This paper presents a review of the activities in digital 3-D imaging in the SWIR (1.5 μm to 1.8 μm) at the National Research Council of Canada. The advantages of the auto-synchronized scanning scheme over conventional triangulation are highlighted. In particular, the laser spot position detection process is reviewed in detail for two types of position detectors that can satisfy different system requirements. Design aspects covering the laser source, optics, and eye-safety considerations are discussed in the context of range imaging. Three-dimensional imaging at a wavelength safe for the human eye has been demonstrated. Because of the excellent signal-to-noise properties of the InGaAs lateral effect photodiode, measurements can be achieved at high resolution using a small fraction of the maximum permissible exposure (MPE). With the availability of more powerful laser sources operating at 1.54 μm, one can foresee the development of high-speed up to video-rate[24], high-resolution, and large volume of view laser scanners[34] for eye safe range imaging. A discussion on the current development of a dual-use range camera intended for space applications is described. This camera combines an InGaAs discrete position detector for triangulation and an avalanche photodiode for a time-of-flight unit. A pulsed laser source emitting at 1.54 μm for eye-safety considerations is used by both ranging devices. Short- (down to 0.5 m) and long-range (several kilometres) measurements will be possible with such a camera.

The design of a vision system for eye safe applications is challenging, since it is concerned with all aspects of evaluation, i.e., image quality and detection processes. It involves the understanding of all system parameters and how they interact to produce results. Rigorous testing should be done to demonstrate that the range cameras are indeed eye safe. At this point the authors have not made any applications to the government agencies concerned. This is an essential step for vision applications that require eye safety, if one wants to speed up the transition of vision systems from laboratory to the space environment or to the factory floor where eye safety is a concern.
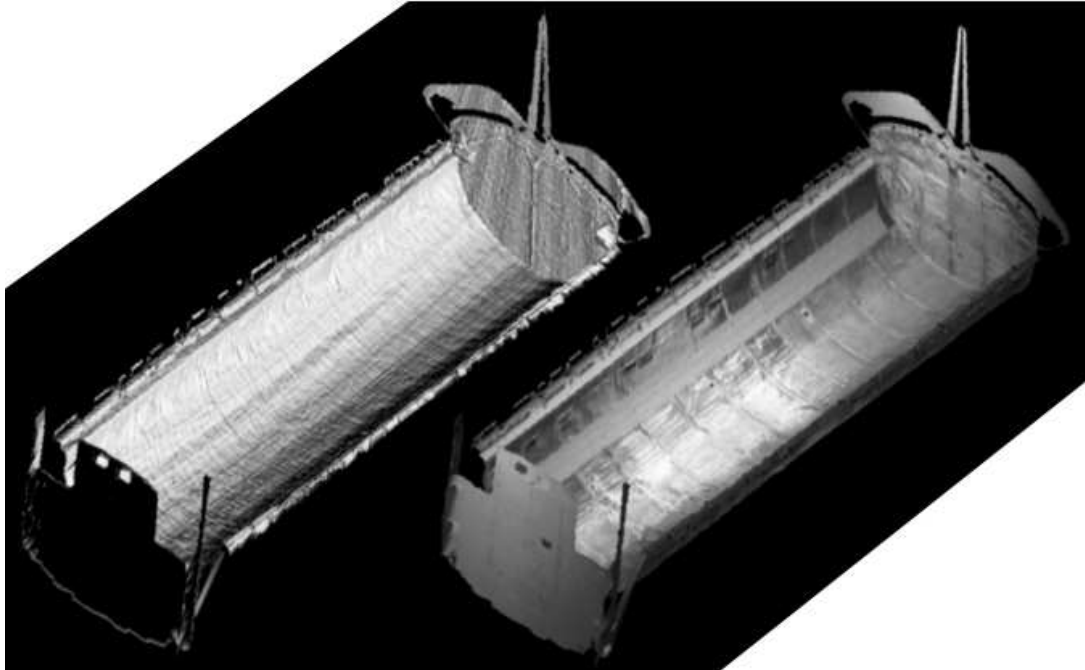
8 Acknowledgments

Figure 12: Orthographic projections of a scaled model of the cargo bay of shuttle (at NRC): (a) shaded, (b) mapping of intensity over shape.

References

[1] M. Rioux, "Applications of Digital 3-D Imaging," Canadian Conf. on Electr. and Comp. Eng., Ottawa, Sept.4-6, 1990, 37.3.1–37.3.10.

[2] P.J. Besl,"Range Imaging Sensors," Machine Vision and Applications, **1**, 127–152 (1988).

[3] M. Rioux, "Laser Range Finder based on Synchronized Scanners," Appl. Opt., **23**, 3837–3844 (1984).

[4] R. Baribeau, M. Rioux and G. Godin,"Color Reflectance Modeling Using a Polychromatic Laser Range Sensor," IEEE Trans. Pattern Anal. Mach. Intell., **14(2)**, 263–269 (1992).

[5] M. D. Nelson, J. F. Johnson and T. S. Lomheim, "General Noise Processes in Hybrid Infrared Focal Plane Arrays," Opt. Eng., **30(11)**, 1682–1700 (1991).

[6] American National Standard for Safe use of Lasers, American National Standards Institute, NY, ANSI Z136.1-1993.

[7] F. Blais, M. Rioux and J.-A. Beraldin,"Practical Considerations for a Design of a High Precision 3-D Laser Scanner System," Proc. Soc. Photo-Opt. Instrum. Eng. **959**, 225–246 (1988).

[8] J.-A. Beraldin, S.F. El-Hakim and L. Cournoyer, "Practical Range Camera Calibration," SPIE Proceedings, Videometrics, **2067**, 21–31 (1993).

[9] J.A. Beraldin, F. Blais, M. Rioux, J. Domey and L. Cournoyer,"Registered Range and Intensity at 10-Mega Samples per Second," Opt. Eng., **31(1)**, 88–94 (1992).

[10] G. Bickel, G. Hausler and M. Maul,"Triangulation with Expanded Range of Depth," Opt. Eng. **24(6)**, 975-977 (1985).

[11] W. Dremel, G. Hausler and M. Maul,"Triangulation with Large Dynamical Range," in Optical Techniques for Industrial Inspection, P.G.Cielo, Ed., Proc. Soc. Photo-Opt. Instrum. Eng. **665**, 182-187 (1986).

[12] R. Baribeau and M. Rioux,"Influence of Speckle on Laser Range Finders ," Appl. Opt. **30**, 2873–2878 (1991).

[13] M.Rioux, G.Bechthold, D.Taylor and M.Duggan,"Design of a Large Depth of View Three-dimensional Camera for Robot Vision,"Opt. Eng. **26(12)**, 1245–1250 (1987).

[14] J.-A. Beraldin,"Design of Bessel-type Pre-Amplifiers for Lateral Effect Photodiodes," Int. J. Electron. **67**, 591–615 (1989).

[15] R. Baribeau and M. Rioux,"Centroid Fluctuations of Speckled Targets," Appl. Opt. **30**, 3752–3755 (1991).

[16] G.H.Olsen,"InGaAs fills the Near-IR Detector-array Vacuum ," Laser Focus World, March A21–A30 (1991).

[17] A.M. Joshi, V.S. Ban, S. Mason and M.J. Lange," 512 and 1024 Element Linear InGaAs Detector Arrays for Near-Infrared (1 μm-3 μm) Environmental Sensing," Proc. Soc. Photo-Opt. Instrum. Eng. **1735**, 287–295 (1992).

[18] F. Blais and M. Rioux, "Real-Time Numerical Peak Detector", Signal Process., **11(2)**,145–155 (1986).

[19] G.M. Borsuk,"Photodetectors for Acousto-Optic Signal Processors", Proc. of the IEEE, **69(1)**,100–118 (1981).

[20] R.W. Simpson,"Noise in Large-aperture Self-scanned Diode Arrays", Rev. Sci. Instrum., **50(6)**, 730–732 (1979).

[21] E.R. Fossum and B. Pain,"Infrared Readout Electronics for Space Science Sensors: State of the Art and Future directions", Infrared Technology XIX, SPIE **2020**, 262–285 (1993).

[22] A.M. Joshi,G.H. Olsen, V.S. Ban and E. Mykietyn,"Popcorn Noise in Linear InGaAs Detector Arrays", Infrared Focal Plane Array Producibility and Related Materials, SPIE **1683**, 200–208 (1992).

[23] P. Maigné, J.-A. Beraldin, T.M. Vanderwel, M. Buchanan and D. Landheer,"An InGaAs/InP Position Sensing Photodetector", IEEE J. of Quantum Electron., **26(5)**, 820–823, (1990).

[24] F.R. Livingstone, L. King, J.-A. Beraldin and M. Rioux,"Development of a Real-Time Laser Scanner System for Object Recognition, Inspection, and Robot Control," SPIE **2057**, 454–461, (1993).

[25] K.S. Kooijman and J.L. Horijon,"Video Rate Laser Scanner: Considerations on Triangulation Optics, Detectors and Processing Circuits," SPIE **2065**, 251–263, (1993).

[26] J.J. Ewing,"Advanced Solid-State Lasers Challenge Conventional Types," Laser Focus World, Nov., 105–110 (1993).

[27] J. Hecht,"Rare Earths Create Useful Long-Wavelength Lasers," Laser Focus World, Nov., 135–142 (1993).

[28] M.S. O'Sullivan, J. Chrostowski, E. Desurvire and J.R. Simpson, "High-power narrow-linewidth Er3+-doped fiber laser," Opt. Lett. 14, **(9)**, 438–440, (1989).

[29] P. Myslinsky, J. Chrostowski, J.A. Koningstein and J.R. Simpson,"High Power Q-Switched Erbium Doped Fiber Laser", IEEE J. of Quantum Electron., **28(1)**, 371–823, (1992).

[30] J. Hecht,"Long-wavelength Diode Lasers are Tailored for Fiberoptics," Laser Focus World, Aug., 79–89 (1992).

[31] D. Nitzan, A.E. Brain and R.O. Duda,"The Measurement and use of Registered Reflectance and Range Data in Scene Analysis," Proc. IEEE, **65(2)**, 206–220 (1977).

[32] G.H. Suits,"Natural Sources," Chap.3 in *The Infrared Handbook* by W.L.Wolfe and G.J. Zissis Editors, ERIM, MI, (1989).

[33] M. Rioux, J.-A. Beraldin, M.S. O'Sullivan and L. Cournoyer,"Eye-Safe Laser Scanner for Range Imaging," Appl. Opt., **30**, 2219–2223 (1991).

[34] F. Blais, J.-A. Beraldin, M. Rioux, R.A. Couvillon, and S.G. MacLean, "Development of a Real-Time Tracking Laser Range Scanner for Space Applications," Workshop on Computer Vision for Space Applications, Antibes, France, Sept. 22–24, 161–171 (1993).